Microchimica Acta (2021) 188:170
https://doi.org/10.1007/s00604-021-04830-0

ORIGINAL PAPER

Electrochemical aptasensor based on Mo_2C/Mo_2N and gold nanoparticles for determination of chlorpyrifos

Zhenfeng Lin[1] · Xin Liu[1] · Yangzi Li[1] · Changxiang Li[1] · Liu Yang[1] · Keke Ma[1] · Zhenwei Zhang[2] · Huayu Huang[1]

Received: 9 December 2020 / Accepted: 12 April 2021

Abstract

Two-dimensional Mo_2C/Mo_2N composites were synthesized by high temperature ball milling and used as support materials for fabricating a chlorpyrifos (CPF) aptasensor. Gold nanoparticles (Au NPs) were electrodeposited on the surface of a Mo_2C/Mo_2N-modified electrode to connect with the ferrocene (Fc) probe via Au–S bonds. The Fc probe can hybridize with the aptamer probe to form a double-stranded structure. The addition of CPF made the double strands melt and the Fc probe approached the surface of the electrode, thereby resulting in amplification of the electrochemical response. The current response of the aptasensor for detecting CPF in solutions linearly varied from 0 to 400 ng mL^{-1} (with a maximum at 0.98 V vs. Ag/AgCl). The Au NPs/Mo_2C/Mo_2N composites exhibited satisfactory electrochemical behavior due to their excellent electrical conductivity and large surface area. This ultrasensitive aptasensor showed a low limit of detection of 0.036 ng mL^{-1}. It was applied to determine CPF in real samples with acceptable recoveries from 94.7 to 116.7%, and the relative standard deviation was from 2.57 to 7.08%.

Keywords Organophosphorus pesticides · Biosensor · Molybdenum nanomaterial · Electrodeposition

Introduction

Pesticides have been crucial for improving grain output [1], but the abuse of pesticides worldwide has caused environmental and food pollution and has been a severe nonnegligible problem [2–4]. Chlorpyrifos (CPF), an effective broad-spectrum insecticide, is one of the most commonly used pesticides in the world. The excessive abuse of CPF has caused a series of hazards to human safety, such as vomiting and convulsions [5]. Consequently, scientists have developed many analytical methods for CPF detection, such as high-performance liquid chromatography [6], gas chromatography-mass spectrometry (GC-MS) [7], continuous flow systems [8], infrared microscopic imaging [9], and thin-layer chromatography [10]. However, detecting CPF at lower concentrations with these methods is difficult. Therefore, the development of ultrasensitive analytical methods for low-abundance CPFs is essential.

Among various methods, electrochemical aptasensors have shown substantial potential in the field of target detection owing to their modification, fast response, and high sensitivity [11]. Aptamers are single-stranded DNA or RNA oligonucleotides that bind targets in vitro through the exponential enrichment ligand system evolution process [12]. Furthermore, aptamers are easy to synthesize, highly accurate, and inexpensive [13], and have been applied to construct biosensors for CPF detection. For example, Sun et al. developed an aptasensor based on mesoporous carbon/multiwalled carbon nanotubes for detecting CPF with a low limit of detection (LOD, 0.33 ng mL^{-1}) [14]. Huo et al. fabricated composites of copper oxide and single-walled carbon nanotubes to construct a selective CPF aptasensor [15]. Sun et al. reported an aptasensor using carbon black and graphene oxide@Fe_3O_4 composites for the sensitive detection of CPFs [16]. Roushani et al. fabricated a CPF aptasensor by modifying a glassy carbon electrode (GCE) with gold nanorods and aptamer-imprinted polymer [17, 18]. These results demonstrated that the combination of aptamers with the modified materials was powerful. Therefore, an efficient sensing material is required to fabricate aptasensors.

✉ Huayu Huang
huanghy@nwu.edu.cn

[1] Shaanxi Key Laboratory of Earth Surface System and Environmental Carrying Capacity, College of Urban and Environmental Science, Northwest University, Xi'an 710127, China

[2] Linyi Institute of Industrial Technology, Linyi 276000, China

Published online: 23 April 2021

Molybdenum-based materials, as a type of two-dimensional (2D) layer materials, have attracted substantial attention in the field of electrochemical sensors [19]. The molybdenum materials have been used as sensing interfaces to modify the electrodes. Jayavel's group fabricated a MoS_2/CuO electrode for the sensitive detection of glucose [20]. Zhang et al. synthesized Co and N-codoped MoO_2 nanomaterials to detect acetaminophen and 4-aminophenol with LODs of 0.013 μM and 0.012 μM, respectively [21]. Vilian et al. used MoS_2 nanocomposites as the electrochemical platform to detect various biomolecules and hazardous chemicals [22]. However, the lack of functional groups of Mo materials resulted in a weak connection with the DNA probe, thereby restricting their further application in aptasensors. To immobilize the DNA probe on the electrode surface, gold nanoparticles (Au NPs), with satisfactory biocompatibility and high electroconductivity, are often connected with DNA probes via Au-S bonds to build aptasensors [23–25].

Here, we employed Mo_2C/Mo_2N composites as a support platform for sensing. The Mo_2C/Mo_2N composites were synthesized by high energy ball milling. Sodium molybdate and urea are ground in a ball mill and calcined at high temperature under the H_2/N_2 atmosphere. Mo_2C/Mo_2N was combined with Au NPs as a signal enhancement strategy to improve the current response of the sensor. A Fc probe with a sulfhydryl group at its 3′ end can be immobilized on the surface of the Au/Mo_2C/Mo_2N electrode through Au–S bonds and hybridized with an aptamer probe to form a double strand. After the addition of CPF, the aptamer was combined with CPF to form a composite melt the rigid double-strand structure. Then, the Fc group approaches the electrode, increasing the signal response of the aptasensor.

Experimental

Reagents

Chlorpyrifos, Sodium molybdate ($NaMoO_4$), 6-mercapto-1-hexanol (MCH), chloroauric acid tetrahydrate ($HAuCl_4 \cdot 4H_2O$), and Nafion 117 solution were obtained from Aladdin Industrial Corporation (Shanghai, China, https://www.aladdin-e.com). Sodium hydrogen phosphate ($Na_2HPO_4 \cdot H_2O$), monosodium phosphate (NaH_2PO_4), potassium ferricyanide ($K_3Fe(CN)_6$) and potassium ferrocyanide ($K_4Fe(CN)_6$) were purchased from Sinopharm (China, https://www.sinoreagent.com). All synthetic oligonucleotide DNA sequences were provided by Sangon Biotech (Shanghai, China, http://www.sangon.com). The aptamer was designed according to a previous study [15]. Oligonucleotide stock solutions were prepared with a phosphate buffer (PB) and stored at 4 °C. The sequences of the oligonucleotides were as follows:

Fc probe: 5′-(Fc)-ACGATGCGGGTGCCAAGCTT-(CH_2)-(SH)-3′.
Aptamer probe: 5′-CCTGCCACGCTCCGCAAGCT TAGGGTTACG CCTGCAGCGATTCTTGATCG CGCTGCTGGTAATCCTTCTTTAAGCTTGGC ACCCGCATCGT-3′.

Preparation of the Mo_2C/Mo_2N composites

The Mo_2C/Mo_2N composites were synthesized by ball milling at high temperature. Initially, 1 g of $NaMoO_4$ and 8 g of urea were added into a 50 mL ball mill pot. The mixture was milled for 4 h (300 rpm) and calcined at 800 °C under a 5% H_2+N_2 gas atmosphere for 90 min. The gas rate was 100–200 cm^3/min, and the temperature increase rate was 10°C/min. After the heat treatment, all samples were cooled to 400°C, removed from the reactor and cooled to ambient temperature under an argon flow. Then, the product was rinsed with deionized water, centrifuged and dried in air at 85°C for 12 h. Mo_2C/Mo_2N (5 mg) was dispersed in 5 mL deionized water by ultrasonic mixing for 30 min. The resulting uniformly dispersed mixture was stored and used for further electrode modification.

Fabrication of the CPF aptasensor

The bare GCE (3-mm diameter) was polished by 0.3 μm and 0.05 μm aluminum slurries, sequentially sonicated separately with deionized water and ethanol for 5 min to remove the residual particles, and dried at room temperature. Ten-microliter Nafion solution (0.05 wt%) was added to 1 mL Mo_2C/Mo_2N suspension to prevent material from falling off the electrode [24], and the mixture was sonicated for 30 min. Ten microliters of the mixture was dropped on the bare GCE surface to prepare the Mo_2C/Mo_2N/GCE. Next, the Mo_2C/Mo_2N/GCE was immersed in a 0.01 M Na_2SO_4 solution containing 2.5 mM $HAuCl_4$, and the i-t method was used to scan for 300 s at a potential of −0.2 V [26]. Au NPs were deposited on the surface of the electrode to form Au/Mo_2C/Mo_2N/GCE. Afterwards, 10 μL Fc probe (1 μM) was dropped on the Au/Mo_2C/Mo_2N/GCE for 30 min to form a single strand. Later, 10 μL aptamer (1 μM) was added to the electrode and hybridized for 50 min to form a double-stranded structure. Finally, 8 μL 1 mM MCH was covered on the electrode for 1 h to block the unreacted sites, resulted in the formation of MCH/Apt/Fc/Au/Mo_2C/Mo_2N/GCE. After each modification step, the electrode was rinsed with 0.1 M PB (pH = 7.0) to remove unconnected residues.

Preparation of the real samples

The feasibility of the sensor was evaluated by detecting CPF in real samples. The apple and pakchoi samples were purchased at a local store and were selected as the specimens for detection. The samples were treated according to the following procedure: The apple and pakchoi were pureed in a blender and centrifuged for 30 min at 2000 rpm to obtain a supernatant. Prior to use, the supernatant was extracted and filtered through a 0.45-μm membrane. The chlorpyrifos reagent was dissolved in anhydrous ethanol (1 μg mL^{-1}) and treated with ultrasound for 30 min. Then, the supernatant was mixed with PB at 1:1 (v:v) ratio and used to dilute CPF solution to obtain 10, 40, 100 and 400 ng mL^{-1}. The real sample solution was tested via differential pulse voltammetry (DPV), and the results were compared with those of GC-MS analysis.

Results and discussion

Characterization of the Mo_2C/Mo_2N composites and Au NPs/Mo_2C/Mo_2N

Figure 1 presents the X-ray diffraction (XRD) pattern of Mo_2C/Mo_2N. The diffraction peaks located at 37.3°, 63.1°, 75.7°, and 79.7° correspond to the (111), (220), (311), and (222) planes, respectively, of Mo_2N (JCPDS card no. 25-1366). The diffraction peaks at 34.3°, 37.9°, 39.3°, 61.5°, and 74.6° correspond to the (100), (002) (101), (110), and (112) planes, respectively, of Mo_2C (JCPDS card no. 35-0787). Mo_2C/Mo_2N was also characterized by electron microscopies (Fig. S1), energy dispersive spectrometry (Fig. S2), and EDS elemental mapping (Fig. S3).

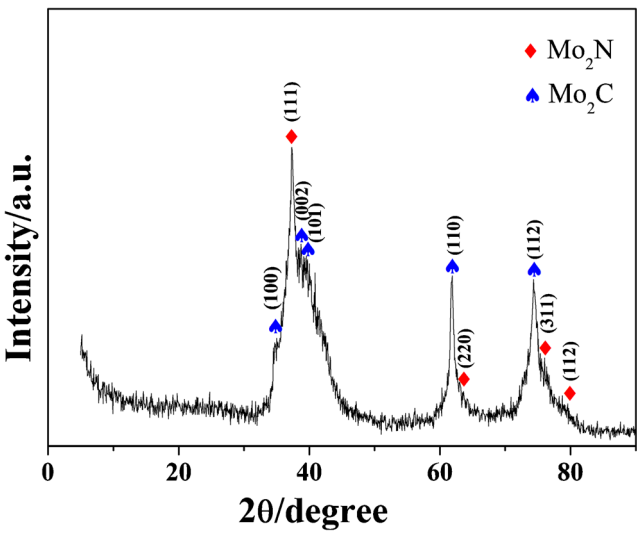

Fig. 1 XRD patterns of Mo_2C/Mo_2N

Electrochemical characterization

The assembly process of the MCH/Apt/Fc/Au/Mo_2C/Mo_2N/GCE was examined via CV and electrochemical impedance spectroscopy (EIS). CV was used to examine modified the electrodes in a 5.0 mM $[Fe(CN)_6]^{3-/4-}$ solution containing 0.1 M KCl at a scan rate of 50 mV/s. In Fig. S4, a reversible CV curve was measured on the bare electrode from −0.4 to 0.6 V (curve a). After the modification of Mo_2C/Mo_2N and deposition of Au NPs (curve b and curve c), the peak current significantly increased compared with the bare GCE. Thus, Mo_2C/Mo_2N increased the surface area to provide more reaction sites, and Au NPs promoted the electron transfer of the electrode. According to the Randles-Sevcik equation:

$$i_p = 2.69 \times 10^5 n^{3/2} A D^{1/2} C_0 v^{1/2}$$

where i_p is the peak current, n is the number of electrons participating in the redox reaction, D_0 is the diffusion coefficient of the molecule in a solution, C_0 is the bulk concentration of the redox probe, A is the electrode surface area, and v is the potential scan rate. The value of bare GCE, Mo_2C/Mo_2N/GCE and Au/Mo_2C/Mo_2N/GCE were calculated to be 0.07, 0.14, and 0.18 cm^2, respectively.

Compared with curve c, the Fc probe and aptamer significantly reduced the CV peak current. Hence, the Fc probe and aptamer hybridized on the surface of the electrode and formed an insulative layer to hinder electron transfer. The peak current of CV decreased after MCH blocked the nonspecific sites because the formed MCH layer hindered the electron transfer between

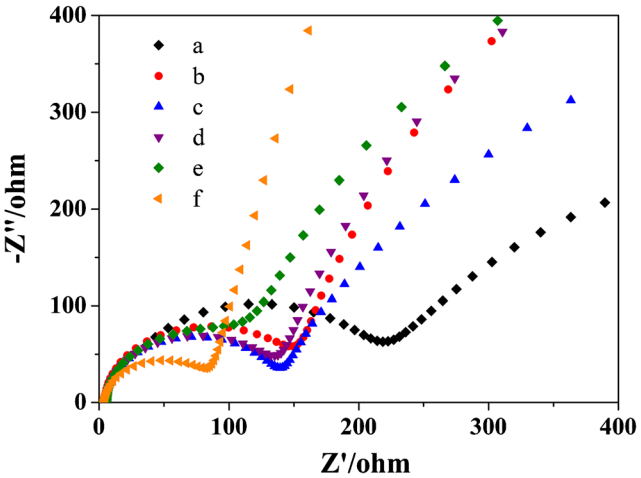

Fig. 2 EIS results with a 5.0-mM $[Fe(CN)_6]^{3-/4-}$ and 0.1 M KCl solution for the following electrodes: **a** the bare GCE, **b** the Mo_2C/Mo_2N/GCE, **c** the Au/Mo_2C/Mo_2N/GCE, **d** the Fc/Apt/Au/Mo_2C/Mo_2N/GCE, **e** the MCH/Fc/Apt/Au/Mo_2C/Mo_2N/GCE, and **f** the MCH/Fc/Apt/Au/Mo_2C/Mo_2N/GCE after incubation with 400 ng mL^{-1} CPF

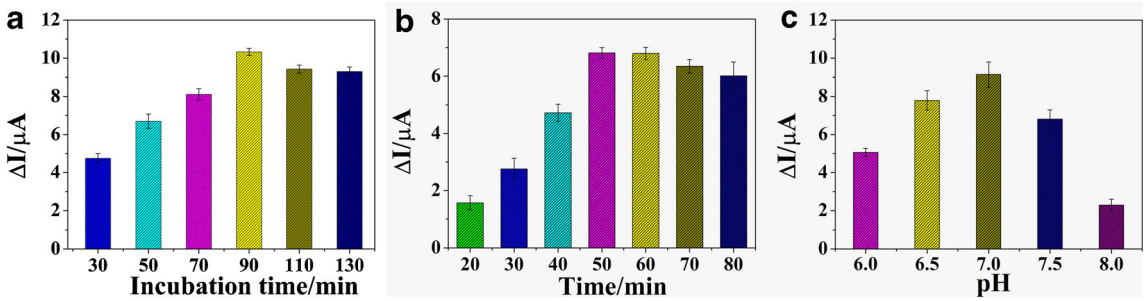

Fig. 3 Optimization of the assay conditions: **a** the aptamer and Fc probe incubation time, **b** the incubation time of the target molecule, and **c** the pH value

$[Fe(CN)_6]^{3-/4-}$ and the electrode (curve e). After the addition of CPF, the electrochemical signal substantially increased (curve f) because aptamers detached from the surface of the electrode.

EIS is an effective tool for characterizing the feature changes in the electrodes. Figure 2 shows the impedance spectra in the Nyquist plots of each assembly process. The electron transfer resistance (R_{et}) is represented by the semicircle diameter of the Nyquist diagram. The trend of EIS characterization results of each electrode is consistent with CV results, demonstrating the complete preparation of the MCH/Apt/Fc/Au/Mo_2C/Mo_2N/GCE.

Optimization of the analytical conditions

To realize electrochemical behavior of the aptasensor, several factors were investigated, including the pH value of the electrolyte, hybridization time of the aptamer and Fc probe, and incubation time with CPF. Figure 3a shows the effect of the hybridization time between aptamer probe and the Fc probe. With increasing hybridization time, the electrochemical signal gradually increased from 30 to 130 min and reached a maximum at 90 min. These results demonstrate the hybridization of aptamer probe with the Fc probe reached a saturation state. Therefore, 90 min was identified as the optimal hybridization time for later studies.

The incubation time with CPF also affected the performance of the aptasensor. The peak current increased with increasing incubation time from 20 to 50 min and slightly decreased with more time eventually. Hence, the accumulation of CPF on the MCH/Apt/Fc/Au/Mo_2C/Mo_2N/GCE surface reached a saturated level (Fig. 3b). Therefore, 50 min was identified as the optimal CPF incubation time.

The effect of the PB pH value was investigated as a parameter in the range of 6.0–8.5. The DPV peak current increased from pH 6.0 to pH 7.0, reached a maximum at pH 7.0, and subsequently gradually decreased (Fig. 3c). The high PB pH value destroyed the stability and activity of immobilized biomolecules, thereby affecting the lifetime of the aptasensor. Consequently, the optimized pH value of PB for the aptasensor was 7.0.

Electrochemical response and calibration curves

The performance of the fabricated aptasensor was investigated with various concentrations of CPF under the optimized conditions (the hybridization time of aptamer probe and the Fc probe was 90 min; the CPF incubation time was 50 min; the pH value of PB was 7.0). In Fig. 4a, the DPV peak current signal gradually increased as the concentration of CPF increased from 0 to 400 ng mL^{-1}. Figure 4b shows a satisfactory linear relationship between the peak current and the logarithmic value of the CPF concentration, and the linear calibration equation is $I = 3.1381 \log C + 5.1239$ ($R = 0.9904$). The LOD of CPF is 0.036 ng mL^{-1} (the calculation equation was $LOD = 3S_a/b$, where S_a is the standard deviation of the blank response and b is the slope of the regression curve) [27]. Table 1 shows a comparison of the MCH/Apt/Fc/Au/Mo_2C/Mo_2N/GCE aptasensor with other electrochemical CPF

Table 1 Comparison of the aptasensor with other reported sensors

Assay	Linear range (ng mL^{-1})	LOD (ng mL^{-1})	Reference
AChE/Au	$4–2.4\times10^4$	1	[28]
PEDOT/GCE	0.35–259.69	0.29	[29]
MIP/Polypyrrole/PGCE	20–300	4.5	[30]
CdS/Graphe/AChE/CHIT/GCE	$2–2\times10^6$	0.7	[31]
Apt/GO@Fe_3O_4/CB/GCE	$0.1–10^5$	0.033	[16]
Apt/OMC-CS/FC@MWCNTS-CS/GCE	$0.1–10^5$	0.33	[14]
MCH/Apt/Fc/Au/Mo_2C/Mo_2N/GCE	0.1–400	0.036	This work

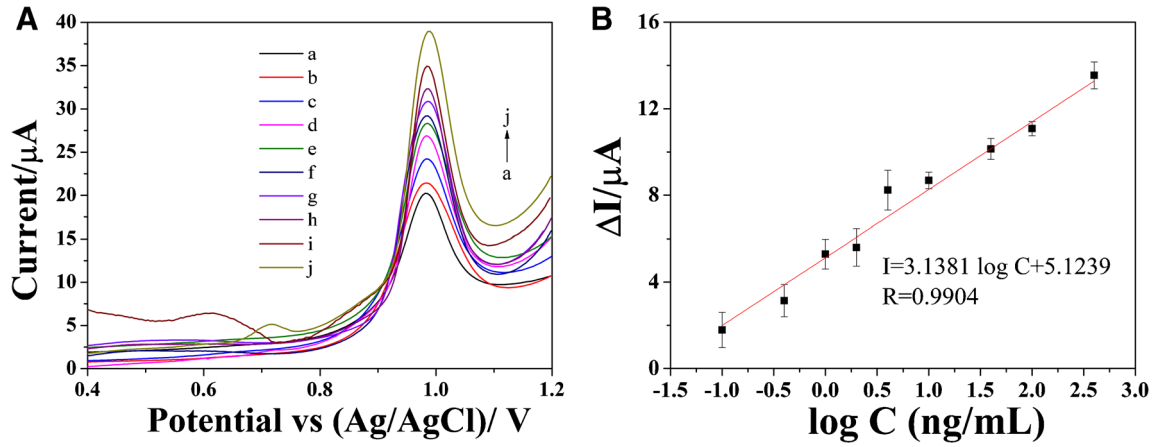

Fig. 4 **a** DPV signals of CPF detection on the prepared sensor with various concentrations (**a**–**j** 0, 0.1, 0.4, 1, 2, 4, 10, 40, 100, and 400 ng mL^{-1}). **b** The linear relationship with the concentration of CPF

sensors. As shown in Table 1, compared with the electrochemical sensor based on quantum dots, molecular imprinting and polymers, molybdenum-based electrochemical sensor has a more competitive LOD. The aptasensor realizes satisfactory performance in CPF detection. Nevertheless, Sun et al. prepared carbon black and graphene oxide@Fe_3O_4 composites to fabricate a sensor for detecting chlorpyrifos and obtained a detection limit of 0.033 ng mL^{-1} [16], still closed to the LOD of 0.036 ng mL^{-1} in the present analytical method. The CPF aptasensor also achieves excellent detection performance. The 2D morphological structure of Mo_2C/Mo_2N provides a large specific surface area. By coupling the Mo_2C/Mo_2N and Au NPs as the supporting electrode material, the excellent biocompatibility and conductivity of composite material improve the sensitivity and stability of the aptasensor. In addition, the proximity of the redox probe Fc to the GCE surface is beneficial to improve the electrochemical redox efficiency of Fc.

Selectivity, stability, and reproducibility

To assess the selectivity of the aptasensor, four pesticides (amitrole, carbendazim, atrazine, and fenitrothion) were used as interfering substances to investigate the selectivity of this aptasensor. The CPF concentration was maintained at 100 ng mL^{-1}, and those of the interfering pesticides were maintained at 1 μg mL^{-1}. As shown in Fig. 5, the results demonstrate this aptasensor has a high specific selectivity for the CPF detection due to the high-specificity binding of aptamer. CPF shows more obvious competitiveness compared with other pesticides.

The reproducibility of the aptasensor was evaluated by fabricating five MCH/Apt/Fc/Au/Mo_2C/Mo_2N/GCEs to detect CPF under the identical experimental conditions. The relative standard deviation (RSD) of the five measurements was 5.62% ($n = 5$), suggesting an acceptable reproducibility of the aptasensor. By storing the MCH/Apt/Fc/Au/Mo_2C/Mo_2N/GCEs at 4 °C for 1 week, the DPV current signal remained at 92.3% to 94.7% ($n = 10$) of its initial response, demonstrating the satisfactory stability of this aptasensor.

Real-sample analysis

To investigate the practical application of the sensor, the MCH/Apt/Fc/Au/Mo_2C/Mo_2N/GCE was used to detect CPF in the apple and pakchoi samples. Initially, no detectable CPF was present in these two samples. Then, CPF was added to the apple and pakchoi samples to obtain the final concentrations of 10, 40, 100, and 400 ng mL^{-1}. According to the regulations of World Health Organization and Food and Agriculture

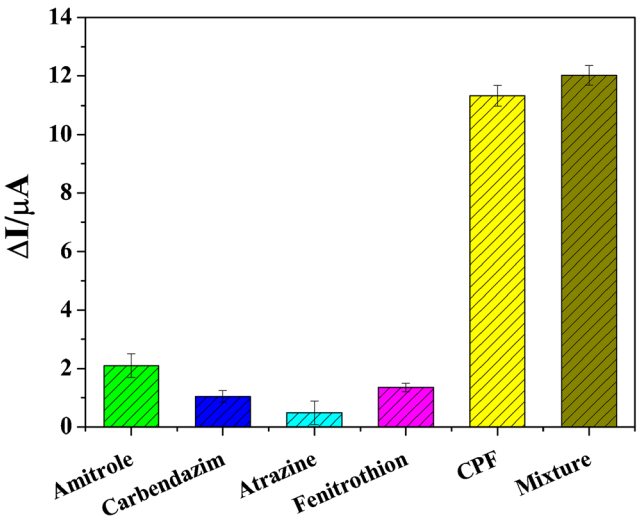

Fig. 5 Selectivity evaluation of the aptasensor detection of amitrole, carbendazim, atrazine, fenitrothion, CPF, and the mixture consisting of the above interference and CPF

Table 2 Detection of CPF in real samples of apple and pakchoi

Sample	Added (ng mL^{-1})	Aptasensor			GC-MS		
		Found (ng mL^{-1})	Recovery (%)	RSD (%, n=3)	Found (ng mL^{-1})	Recovery (%)	RSD (%, n=3)
Apple	0	Not found	–	–	Not found	–	–
	10.0	11.6±1.44	116.7	6.47	10.2±0.22	101.9	4.02
	40.0	41.6±2.07	104.1	6.81	39.8±0.75	99.7	1.63
	100.0	94.7±2.4	94.7	2.57	101.2±2.3	101.2	2.31
	400.0	409.4±15.4	102.4	3.77	403.6±8.7	100.7	2.17
Pakchoi	0	Not found	–	–	Not found	–	–
	10.0	11.3±1.36	113.6	6.50	9.8±0.37	98.9	3.19
	40.0	39.6±3.19	99.1	7.08	39.8±0.71	99.6	2.09
	100.0	101.6±4.0	101.6	3.95	101.8±2.9	101.8	2.86
	400.0	397.1±23.6	99.2	5.96	399.1±5.1	99.7	1.26

Organization, the maximum residue limit of Chinese cabbage and fruit was 1 mg/kg (http://www.fao.org/fao-who-codexalimentarius/codex-texts/dbs/pestres/pesticide-detail/en/?p_id=17). It is obvious that the sensitivity of the method can reach the detection requirement. The spiked CPF samples were measured via DPV and GC-MS. As presented in Table 2, the CPF recoveries ranged from 94.7 to 116.7%, and the RSD was from 2.57 to 7.08%. There were no significant differences between the aptasensor and GC-MS in the CPF testing. These results demonstrate that this aptasensor has high potential in practical applications.

Conclusions

A CPF aptasensor was developed based on electrodepositing Au NPs on the Mo_2C/Mo_2N electrode surface. The synthesis of Mo_2C/Mo_2N composites requires ball milling of $NaMoO_4$ and urea for several hours and then calcination at high temperature. The size of single Mo_2C/Mo_2N needs to be precisely controlled by the synthesis conditions. The improvement of the $Au/Mo_2C/Mo_2N$ platform demonstrates the synergistic interactions of Mo_2C/Mo_2N and Au NPs. In addition, Fc served as an active group to boost the electron transfer rate for the redox reaction between electrodes and electrolytes. Based on these features, this aptasensor exhibited outstanding performance in the detection of CPF with an LOD of 0.036 ng mL^{-1} and excellent discrimination against other pesticides. Furthermore, the aptasensor has been used to detect CPF in apple and pakchoi samples with satisfactory recoveries. All results regarding the electrochemical features demonstrate that our designed aptasensor has potential application value in the field of CPF detection.

Supplementary Information The online version contains supplementary material available at https://doi.org/10.1007/s00604-021-04830-0.

Acknowledgements This work was supported by the Program for Key Research and Development Plan in Shaanxi Province (No. 2019SF-243), the Innovation Capability Support Program of Shaanxi Province (No. 2020TD-022), and the Strategic Priority Research Program of Chinese Academy of Sciences (XDB40000000).

Compliance with ethical standards

Conflict of interest The authors declare that they have no conflicts of interest.

References

1. Eddleston M, Buckley NA, Eyer P, Dawson AH (2008) Management of acute organophosphorus pesticide poisoning. Lancet 371(9612):597–607. https://doi.org/10.1016/s0140-6736(07)61202-1
2. Carvalho FP (2017) Pesticides, environment, and food safety. Food and Energy Security 6(2):48–60. https://doi.org/10.1002/fes3.108
3. Lewis K, Tzilivakis J, Warner D, Green A (2016) An international database for pesticide risk assessments and management. Hum Ecol Risk Assess 22(4):1050–1064. https://doi.org/10.1080/10807039.2015.1133242
4. Zhou J, Zou X, Song S, Chen G (2018) Quantum dots applied to methodology on detection of pesticide and veterinary drug residues. J Agric Food Chem 66(6):1307–1319. https://doi.org/10.1021/acs.jafc.7b05119
5. Wang P, Dai W, Ge L, Yan M, Ge S, Yu J (2013) Visible light photoelectrochemical sensor based on au nanoparticles and molecularly imprinted poly(o-phenylenediamine)-modified TiO2 nanotubes for specific and sensitive detection chlorpyrifos. Analyst 138(3):939–945. https://doi.org/10.1039/c2an36266j
6. He L, Luo X, Xie H, Wang C, Jiang X, Lu K (2009) Ionic liquid-based dispersive liquid-liquid microextraction followed high-performance liquid chromatography for the determination of organophosphorus pesticides in water sample. Anal Chim Acta 655(1):52–59. https://doi.org/10.1016/j.aca.2009.09.044

7. Sinha SN, Pal RR, Dewan A, Mansuri MM, Saiyed HN (2006) Effect of dissociation energy on ion formation and sensitivity of an analytical method for determination of chlorpyrifos in human blood, using gas chromatography–mass spectrometer (GC–MS in MS/MS). Int J Mass Spectrom 253(1):48–57. https://doi.org/10.1016/j.ijms.2006.02.020
8. Jeanty G, Ghommidh C, Marty J (2001) Automated detection of chlorpyrifos and its metabolites by a continuous flow system-based enzyme sensor. Anal Chim Acta 436(1):119–128. https://doi.org/10.1016/S0003-2670(01)00898-4
9. Li X, Zhang W, Wu X, Sun C, Chen M, Zeng Q (2012) Mucoepidermoid carcinoma of the lung: common findings and unusual appearances on CT. Clin Imaging 36(1):8–13. https://doi.org/10.1016/j.clinimag.2011.03.003
10. Li S, Liang W, Zheng F, Lin X, Cai J (2014) Ascorbic acid surface modified TiO2-thin layers as a fully integrated analysis system for visual simultaneous detection of organophosphorus pesticides. Nanoscale 6(23):14254–14261. https://doi.org/10.1039/C4NR04430D
11. Akyuz D, Keles T, Biyiklioglu Z, Koca A (2017) Electrochemical pesticide sensors based on electropolymerized metallophthalocyanines. J Electroanal Chem 804:53–63. https://doi.org/10.1016/j.jelechem.2017.09.044
12. Famulok M, Hartig JS, Mayer G (2007) Functional aptamers and aptazymes in biotechnology, diagnostics, and therapy. Chem Rev 107(9):3715–3743. https://doi.org/10.1021/cr0306743
13. Zhu L, Liu Y, Yang P, Liu B (2015) Label-free Aptasensor based on electrodeposition of gold nanoparticles on graphene and its application in the quantification of adenosine triphosphate. Electrochim Acta 172:88–93. https://doi.org/10.1016/j.electacta.2015.04.100
14. Jiao Y, Jia H, Guo Y, Zhang H, Wang Z, Sun X, Zhao J (2016) An ultrasensitive aptasensor for chlorpyrifos based on ordered mesoporous carbon/ferrocene hybrid multiwalled carbon nanotubes. RSC Adv 6(63):58541–58548. https://doi.org/10.1039/c6ra07735h
15. Xu G, Huo D, Hou C, Zhao Y, Bao J, Yang M, Fa H (2018) A regenerative and selective electrochemical aptasensor based on copper oxide nanoflowers-single walled carbon nanotubes nanocomposite for chlorpyrifos detection. Talanta 178:1046–1052. https://doi.org/10.1016/j.talanta.2017.08.086
16. Jiao Y, Hou W, Fu J, Guo Y, Sun X, Wang X, Zhao J (2017) A nanostructured electrochemical aptasensor for highly sensitive detection of chlorpyrifos. Sensors Actuators B Chem 243:1164–1170. https://doi.org/10.1016/j.snb.2016.12.106
17. Roushani M, Nezhadali A, Jalilian Z (2018) An electrochemical chlorpyrifos aptasensor based on the use of a glassy carbon electrode modified with an electropolymerized aptamer-imprinted polymer and gold nanorods. Microchim Acta 185(12):551. https://doi.org/10.1007/s00604-018-3083-0
18. Rohaizad N, Mayorga-Martinez CC, Sofer Z, Pumera M (2017) 1T-phase transition metal dichalcogenides (MoS2, MoSe2, WS2, and WSe2) with fast heterogeneous electron transfer: application on second-generation enzyme-based biosensor. ACS Appl Mater Interfaces 9(46):40697–40706. https://doi.org/10.1021/acsami.7b13090
19. Arunbalaji S, Vasudevan R, Arivanandhan M, Alsalme A, Alghamdi A, Jayavel R (2020) CuO/MoS2 nanocomposites for rapid and high sensitive non-enzymatic glucose sensors. Ceram Int 46(10):16879–16885. https://doi.org/10.1016/j.ceramint.2020.03.265
20. Dong Y, Zhou M, Zhang L (2019) 3D multiporous Co,N co-doped MoO2/MoC nanorods hybrids as improved electrode materials for highly sensitive simultaneous determination of acetaminophen and 4-aminophenol. Electrochim Acta 302:56–64. https://doi.org/10.1016/j.electacta.2019.02.006
21. Xiao T, Huang J, Wang D, Meng T, Yang X (2020) Au and Au-based nanomaterials: synthesis and recent progress in electrochemical sensor applications. Talanta 206:120210–120210. https://doi.org/10.1016/j.talanta.2019.120210
22. Vilian ATE, Dinesh B, Kang SM, Krishnan UM, Huh YS, Han YK (2019) Recent advances in molybdenum disulfide-based electrode materials for electroanalytical applications. Mikrochim Acta 186(3):203. https://doi.org/10.1007/s00604-019-3287-y
23. Razavipanah I, Rounaghi GH, Deiminiat B, Damirchi S, Abnous K, Izadyar M, Khavani M (2019) A new electrochemical aptasensor based on MWCNT-SiO2@au core-shell nanocomposite for ultrasensitive detection of bisphenol a. Microchem J 146:1054–1063. https://doi.org/10.1016/j.microc.2019.02.018
24. Zhu C, Liu D, Chen Z, Li L, You T (2019) An ultra-sensitive aptasensor based on carbon nanohorns/gold nanoparticles composites for impedimetric detection of carbendazim at picogram levels. J Colloid Interface Sci 546:92–100. https://doi.org/10.1016/j.jcis.2019.03.035
25. McGovern MS, Garnett EC, Rice C, Masel RI, Wieckowski A (2003) Effects of Nafion as a binding agent for unsupported nanoparticle catalysts. J Power Sources 115(1):35–39. https://doi.org/10.1016/s0378-7753(02)00623-7
26. Sun X, Zhu Y, Wang X (2012) Amperometric immunosensor based on deposited gold nanocrystals/4,4′-thiobisbenzenethiol for determination of carbofuran. Food Control 28(1):184–191. https://doi.org/10.1016/j.foodcont.2012.04.027
27. Desimoni E, Brunetti B (2013) Presenting analytical performances of electrochemical sensors. Some suggestions. Electroanalysis 25(7):1645–1651. https://doi.org/10.1002/elan.201300150
28. Li Y, Gan Z, Li Y, Liu Q, Bao J, Dai Z, Han M (2010) Immobilization of acetylcholinesterase on one-dimensional gold nanoparticles for detection of organophosphorous insecticides. Science China Chem 53(4):820–825. https://doi.org/10.1007/s11426-010-0105-0
29. Manisankar P, Viswanathan S, Pusphalatha AM, Rani C (2005) Electrochemical studies and square wave stripping voltammetry of five common pesticides on poly 3,4-ethylenedioxythiophene modified wall-jet electrode. Anal Chim Acta 528(2):157–163. https://doi.org/10.1016/j.aca.2004.08.027
30. Uygun ZO, Dilgin Y (2013) A novel impedimetric sensor based on molecularly imprinted polypyrrole modified pencil graphite electrode for trace level determination of chlorpyrifos. Sensors Actuators B Chem 188:78–84. https://doi.org/10.1016/j.snb.2013.06.075
31. Wang K, Liu Q, Dai L, Yan J, Ju C, Qiu B, Wu X (2011) A highly sensitive and rapid organophosphate biosensor based on enhancement of CdS-decorated graphene nanocomposite. Anal Chim Acta 695(1–2):84–88. https://doi.org/10.1016/j.aca.2011.03.042